Mott Physics and Topological Phase Transition in Correlated Dirac Fermions

Shun-Li Yu,[1] X. C. Xie,[2,3] and Jian-Xin Li[1]

[1]National Laboratory of Solid State Microstructures and Department of Physics, Nanjing University, Nanjing 210093, China
[2]International Center for Quantum Materials, Peking University, Beijing 100871, China
[3]Department of Physics, Oklahoma State University, Stillwater, Oklahoma 74078

(Received 2 January 2011; revised manuscript received 27 May 2011; published 29 June 2011)

We investigate the interplay between the strong correlation and the spin-orbit coupling in the Kane-Mele-Hubbard model and obtain the qualitative phase diagram via the variational cluster approach. We identify, through an increase of the Hubbard U, the transition from the topological band insulator to either the spin liquid phase or the easy-plane antiferromagnetic insulating phase, depending on the strength of the spin-orbit coupling. A nontrivial evolution of the bulk bands in the topological quantum phase transition is also demonstrated.

DOI: 10.1103/PhysRevLett.107.010401 PACS numbers: 71.10.Pm, 03.65.Vf, 71.27.+a, 71.30.+h

Recently, a new field has emerged in condensed matter physics, based on the realization that a spin-orbit interaction (SOI) can lead to topologically insulating electronic phases [1,2]. A topological band insulator (TBI) has a nontrivial band structure coming from the strong SOI. Theoretical and experimental studies have found such materials in both two (2D) [3–5] and three [6–10] dimensions. TBI is characterized by a charge excitation gap in the bulk, and gapless helical edge (or surface) states lying inside the bulk gap protected by the time reversal symmetry. As a new quantum state which is the Z_2-graded topological distinction from other conventional insulators, it has attracted great attention. Though great progress has been achieved, the current research mostly focuses on the weakly interacting systems. It has been proposed that the topological insulator may also appear in the systems with substantial electron correlations, such as $4d$ and $5d$ transition metal oxides [11,12]. It is also shown experimentally that the electron interaction plays a crucial role in determining the ground state of topological insulators in the 2D limit [13]. Therefore, the effects of electron correlations on the topological insulators present a new challenge.

The correlation effects in topological insulators can be studied either by interaction-driven topological insulators [14–16] or by introducing interactions to a system with a strong SOI [11,17–19]. In this Letter, we investigate the model proposed by Kane and Mele [3] on the honeycomb lattice for describing a 2D topological insulator, and introduce the Hubbard interaction to analyze the Mott physics. Recently, the Hubbard model on the honeycomb lattice has been studied by Meng *et al.* [20] using the quantum Monte Carlo (QMC) method, in which a spin liquid (SL) phase is found to exist between the semimetallic (SM) phase and the antiferromagnetic (AF) Mott insulator (MI) phase. The mean-field analysis and QMC simulations for the Kane-Mele-Hubbard (KMH) model reveal that the TBI phase is unstable against the magnetic ordering phase [17,21,22]. But the whole phase diagram, especially the transition between the TBI and the MI, and the nature of the single-particle excitations in the bulk and on the edges are still open questions. As the existence of gapless edge states is the direct manifestation of the topological nature, the study of the single-particle excitation spectra is the natural way to investigate the phase transition between TBI and MI. Here, we use the variational cluster approach (VCA) [23], which takes into account exactly the effects of short-range correlations by an exact diagonlization of the separative clusters. We find a topological quantum phase transition from TBI to MI or SL with increasing U and this process shows a nontrivial evolution. Starting from TBI, the SOI gap Δ_{SO} closes first and then the Mott gap opens up but without the gapless edge states for increasing U, which is closely related to the topological properties of the system. The closing process of Δ_{SO} is accompanied with a splitting of both the conduction and valence bands. For the strong SOI, the state transiting from TBI is the easy-plane AF Mott insulator. For the weak coupling, a spin liquid phase emerges between the TBI and the AF Mott insulator.

The Kane-Mele-Hubbard model is defined as $H = H_0 + H_U$, where H_0 is the model proposed by Kane and Mele on the honeycomb lattice as shown in Fig. 1(a) [3],

$$H_0 = t\sum_{\langle ij\rangle\sigma} c^{\dagger}_{i\sigma}c_{j\sigma} + i\lambda\sum_{\langle\langle ij\rangle\rangle\sigma\sigma'} \nu_{ij}c^{\dagger}_{i\sigma}\tau^{z}_{\sigma\sigma'}c_{j\sigma'}, \quad (1)$$

and H_U the Hubbard interaction,

$$H_U = U\sum_i n_{i\uparrow}n_{i\downarrow}. \quad (2)$$

Here, $\langle i, j\rangle$ and $\langle\langle ij\rangle\rangle$ denote the nearest neighbor (NN) and the next NN, respectively. λ is the SOI constant and τ the Pauli matrices. $\nu_{ij} = +1(-1)$ if the electron makes a left (right) turn to get to the next NN site. Others are in standard notation. We notice that the model can decouple into two independent Hamiltonians for the up and down spins and each is odd under time reversal. So, it is in the integer quantum Hall (IQH) class.

VCA is a cluster method of the self-energy functional approach [23]. It has been successfully applied to, for instance, the study of competing phases in high-T_c superconductors [24,25]. Despite the considerable finite-size errors, VCA can predict the qualitatively correct trend for the phase diagram [26]. In VCA, the lattice is tiled into superlattice of clusters and the reference system is made up of the decoupled clusters. The single-particle parameters (denoted by $\mathbf{t}'$) of the reference system are optimized according to the variational principle. And one can add any Weiss field to study the symmetry broken phases. For the self-energy parameterized as $\mathbf{\Sigma}'(\mathbf{t}')$, we have the grand potential:

$$\Omega[\mathbf{\Sigma}'(\mathbf{t}')] = \Omega'(\mathbf{t}') + \mathrm{Tr}\ln[-(\mathbf{G}_0^{-1} - \mathbf{\Sigma}'(\mathbf{t}'))^{-1}] - \mathrm{Tr}\ln[-\mathbf{G}'(\mathbf{t}')], \quad (3)$$

where $\Omega'(\mathbf{t}')$ and $\mathbf{G}'(\mathbf{t}')$ are the grand potential and Green's function of the reference system, $\mathbf{G}_0$ is the free Green's function without interactions. The physical self-energy $\mathbf{\Sigma}$ is given by the stationary point $\partial\Omega[\mathbf{\Sigma}'(\mathbf{t}')]/\partial\mathbf{t}' = 0$.

In our calculations, $\mathbf{\Sigma}'(\mathbf{t}')$ is determined by $\mathbf{\Sigma}'(\mathbf{t}') = \mathbf{G}_0^{-1} - \mathbf{G}^{-1}(\mathbf{t}')$ and the lattice Green's function $\mathbf{G}(\mathbf{t}')$ is calculated via the cluster perturbation theory [27]. We first calculate $\mathbf{G}'(\mathbf{t}')$ of each cluster by the exact diagonalization method and then get $\mathbf{G}(\mathbf{t}')$ by treating the inter-cluster hopping $\mathbf{V}$ perturbatively, namely $\mathbf{G}(\mathbf{k}, \omega) = \mathbf{G}'(\mathbf{k}, \omega)[1 - \mathbf{V}(\mathbf{k})\mathbf{G}'(\mathbf{k}, \omega)]^{-1}$ written in the momentum space. Where the matrix $\mathbf{V}$ is given by $V_{\mu\nu}(\mathbf{k}) = \sum_{\mathbf{R}} V_{\mu\nu}^{0\mathbf{R}} e^{i\mathbf{k}\cdot\mathbf{R}}$ with $\mathbf{R}$ the superlattice index. $V_{\mu\nu}^{0\mathbf{R}}$ contains all hopping terms between two clusters at 0 and R, μ and ν denote different sites and spins in the two clusters. For the calculation of bulk states, each cluster consists of a hexagon [see Fig. 1(a)]. For the calculation of edge states, we consider a strip geometry as illustrated in Fig. 1(c). In order to completely tiling the strip, a 12-site cluster is used. In realistic calculations, eight clusters are included in the y direction to form a supercluster and the superclusters are arranged periodically in the x direction. For illustration, we only show schematically two superclusters in the y direction in Fig. 1(c). We have checked the results for ribbons with different widths and with different cluster sizes in the calculation of edge states, and find no obvious quantitative changes.

To test the existence of the possible AF order, we will include the following Weiss field, $H_{\mathrm{AF}}^{\alpha} = h_{\mathrm{AF}}^{\alpha}\sum_i (-1)^{\eta_i} c_{i\sigma}^{\dagger}\tau_{\sigma\sigma'}^{\alpha} c_{i\sigma'}$, where $\eta_i = 0$ or 1, when $i \in A$ or B. In the absence of the SOI, the spin sector has a $SU(2)$ symmetry. So, we have $h_{\mathrm{AF}}^{z} = h_{\mathrm{AF}}^{x,y}$. This relation is broken when the SOI is turned on. In this case, we will calculate the grand potential $\Omega(h_{\mathrm{AF}})$ as a function of h_{AF}^{z} and h_{AF}^{x}, respectively.

Our main results on the interplay between the Hubbard interaction and the SOI are summarized in the $U - \lambda$ phase diagram [Fig. 2]. Let us first discuss the $\lambda = 0$ line.

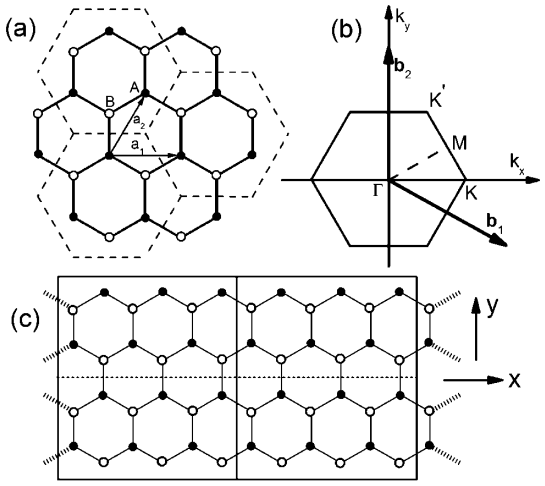

FIG. 1. (a) 6-site cluster tiling (dashed lines) on honeycomb lattice used for the calculations of bulk properties. A and B denote the two inequivalent sites, $\mathbf{a}_1$ and $\mathbf{a}_2$ the lattice unit vectors. (b) First Brillouin zone. (c) An illustration of tiling the ribbon used for the calculations of edge states. The superlattices (rectangle with solid lines) are arranged periodically along the x direction. For illustration, we only plot two clusters (separated by the dotted horizontal line) in each superlattice, while in the calculations eight clusters are included.

In VCA, the existence of the AF order can be determined by the h_{AF}^{α} dependence of the grand potential $\Omega(h_{\mathrm{AF}})$. Figure 3(a) presents the results for different U. For weak U, such as $U = 2t$ and $4t$, $\Omega(h_{\mathrm{AF}})$ shows a monotonic increase with h_{AF}^{z} ($h_{\mathrm{AF}}^{z} = h_{\mathrm{AF}}^{x}$ in this case), indicating that no AF order forms in the system. However, for a large U such as $U \geq 6t$, a minimum appears at finite h_{AF}^{z} and this minimum moves to lower h_{AF}^{z} values with increase of U. Therefore, we can infer that an AF order exists for a large U as expected. Interestingly, we find that an obvious Mott gap has opened up around the Fermi energy in the density of states at $U = 4t$ [Fig. 3(b)]. This paramagnetic insulating phase is identified as the SL phase as also been found recently by Meng *et al.* using the QMC simulation [20].

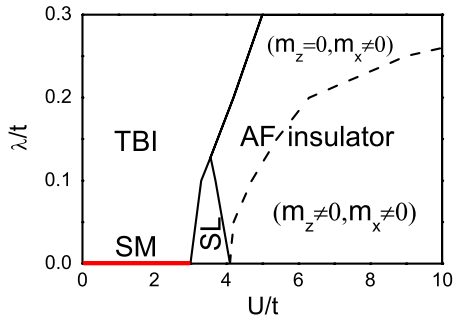

FIG. 2 (color online). Qualitative phase diagram of KMH model. SM, TBI, SL and AF insulator denote the semimetal, topological band insulator, spin liquid and antiferromagnetic insulator, respectively. Above the dashedline in the AF insulator phase, the z term of the AF order disappears.

Therefore, the system will undergo phase transitions from the SM to SL and then to AF Mott insulator with U. Thus, we can reproduce the QMC simulation results calculated for $\lambda = 0$ [20].

When turning on the SOI, we find that the SL phase maintains for a range of SOI up to $\lambda = 0.125t$. On the other hand, the AF order is not isotropic. As seen from Figs. 3(c) and 3(d), no minimum is found at $U = 4t$ for $\lambda = 0.2t$ in the h^z_{AF} dependence, but it can be found in the h^x_{AF} dependence. It indicates that within a range of U, the z-direction AF order is destroyed once the SOI is present. For $\lambda < 0.25t$, when increasing U further, we find the appearance of the z-term in the AF order eventually. However, for $\lambda \geq 0.25t$, it has not been found up to $U = 10t$. Thus, in the phase diagram we plot the dashed line separating the AF order with and without the z term. The easy-plane AF order is the result of the interplay between the Hubbard interaction and the SOI. As well known, the NN hopping will generate an isotropic AF Heisenberg term $H_1 = J_1 \sum_{\langle ij \rangle} \mathbf{S}_i \cdot \mathbf{S}_j$ with $J_1 = 4t^2/U$ in the strong-coupling limit. Similarly, the next NN SOI generates an anisotropic exchanging term $H_2 = J_2 \sum_{\langle\langle ij \rangle\rangle} (-S^x_i S^x_j - S^y_i S^y_j + S^z_i S^z_j)$ [17], with $J_2 = 4\lambda^2/U$. Notice that the z term in H_2 favors antiparallel alignment of the spins on the next NN sites; thus, it will introduce a frustration to the NN AF correlation expressed by H_1. On the other hand, the xy term in H_2 favors a ferromagnetic alignment, so no frustration is introduced. As a result, H_2 coming from the SOI will suppress the z-term of the AF order.

At another limit $U = 0$, a TBI is expected to occur once the SOI is turned on [3]. The TBI is characterized by gapless edge states protected by the bulk gap opened by the SOI. The spectral function of single particles is given by $A(\mathbf{k}, \omega) = -2\,\mathrm{Im}G(\mathbf{k}, \omega)/\pi$. The results for several U at $\lambda = 0.1t$ are presented in Fig. 4, where the bulk bands are plotted along the lines shown in Fig. 1(b) and the edge states are calculated from a ribbon with the zigzag edges [Fig. 1(c)]. For $U = 0$, one can see that a bulk gap opens resulting from the SOI [Fig. 4(a)]. At the meantime, clear gapless edge states with sizeable spectral weights emerge [Fig. 4(b)]. These results reproduce perfectly the characters of a TBI [3]. Turning on the Hubbard interaction U, we find that the bulk gap is reduced firstly and the edge states are stable against a weak U, as shown in Figs. 4(c)–4(f). When U is increased further, the bulk gap closes and the edge states disappear simultaneously. After that, a bulk gap with the character of the Mott gap occurs and no edge states reemerge anymore, as shown in Figs. 4(g) and 4(h). Thus,

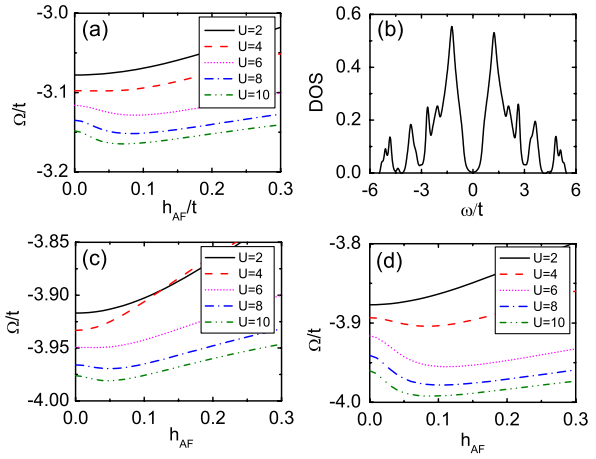

FIG. 3 (color online). (a) Ω as a function of h_{AF} for various values of U at $\lambda = 0$. (b) The density of states for $U = 4$ and $\lambda = 0$. (c) and (d): Ω vs h_{AF} at $\lambda = 0.2t$ along the z and x-directions, respectively.

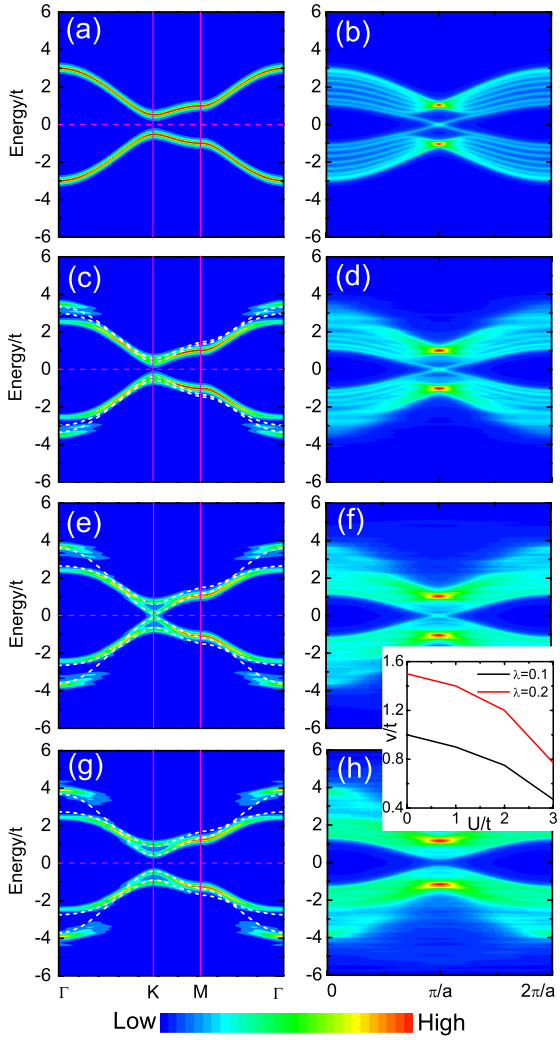

FIG. 4 (color online). Intensity plot of $A(\mathbf{k}, \omega)$ for single-particle excitations in the bulk [Figs. (a), (c), (e) and (g)] and in the ribbon with the zigzag edges [Figs. (b), (d), (f) and (h)] at $\lambda = 0.1t$. The white dashed curves in Figs. (c), (e) and (g) are the mean-field fits discussed in the text. From the up to down figures, $U = 0, 2t, 3t, 4t$. The colors represent the intensity of spectrum function as indicated by the color scale at the bottom. The inset shows the U dependence of the renormalized velocity of edge states at $\lambda = 0.1t$ and $0.2t$.

we determine the phase boundary where the TBI disappears by a criteria that the bulk gap closes and the edge states disappear. Combining the above results, we conclude that the TBI phase will make transition to the SL phase when $\lambda \leq 0.125t$ and to the easy-xy plane AF phase for $\lambda > 0.125t$, as presented in the phase diagram of Fig. 2.

According to the bulk-boundary correspondence [1], the existence of gapless edge states depends on the topological class of the bulk band structure. The transition from TBI (topologically nontrivial state) to MI (toplogically trivial state) must undergo a gap closing process in the bulk. As far as we know, this process is demonstrated clearly for the first time by a systematic numerical calculation presented here.

A first attempt to understand the evolution of the spectrums in the KMH model is to include the AF order parameter $m^A = -m^B = |\langle n_{i\uparrow} - n_{i\downarrow}\rangle|$ [A and B denote the sublattice in Fig. 1(a)] [17]. This gives rise to the mean-field dispersion given by $E(\mathbf{k}) = \pm\sqrt{\varepsilon^2(\mathbf{k}) + (\lambda - Um/2)^2}$, with $\varepsilon(\mathbf{k})$ the bare dispersion. When $Um/2 = \lambda$, the spin-orbit gap closes. Then another gap $Um/2 - \lambda$ with a character of the Mott gap opens up with the further increase of U. However, the evolution shown in Fig. 4 exhibits a more complex behavior, namely, both the valence and conduction bands around K are split into two subbands. Comparing the numerical results for different U and λ, we note that the band splitting around K depends on λ^2/U. This is the exchange integral in H_2 coming from the second-order process of the spin-orbit interaction as described above. So, we rewrite H_2 as [17] $H_\lambda^{(2)} = -(J_2/2)\sum_{\langle\langle ij\rangle\rangle}(a_{i\uparrow}^\dagger a_{j\uparrow} - a_{i\downarrow}^\dagger a_{j\downarrow})(a_{j\uparrow}^\dagger a_{i\uparrow} - a_{j\downarrow}^\dagger a_{i\downarrow})$ and choose another parameter $\chi = \langle a_{i\uparrow}^\dagger a_{j\uparrow} - a_{i\downarrow}^\dagger a_{j\downarrow}\rangle$. By using m^A and χ as adjustable parameters, we can give a fit to the numerical results, which is plot as white dashed lines in Fig. 4. This simple fit provides a possible understanding of the evolution of the bulk bands.

Finally, let us discuss the effect of electron correlations on the edge states. As shown in the inset of Fig. 4, we notice a visible reduction of the velocity in helical Dirac fermions at the edge in the TBI phase. This renormalization arising from the two-particle scattering between the left and right moving modes due to electron correlations, which is allowed by the time reversal symmetry [28,29].

In summary, we have investigated the interplay between the Hubbard interaction and the spin-orbit coupling in the Kane-Mele-Hubbard model with the variational cluster approach. We map a detail $U - \lambda$ phase diagram, in which the topological band insulator, the spin liquid, and the antiferromagnetic insulator are identified.

This work is supported by NSF-China and the MOST-China. XCX is also supported by US-DOE through the grant DE-FG02-04ER46124.

[1] M. Z. Hasan and C. L. Kane, Rev. Mod. Phys. **82**, 3045 (2010).
[2] X. L. Qi and S. C. Zhang, arXiv:1008.2026.
[3] C. L. Kane and E. J. Mele, Phys. Rev. Lett. **95**, 146802 (2005); C. L. Kane and E. J. Mele, Phys. Rev. Lett. **95**, 226801 (2005).
[4] B. A. Bernevig, T. A. Hughes, and S. C. Zhang, Science **314**, 1757 (2006).
[5] M. König *et al.*, Science **318**, 766 (2007).
[6] D. Hsieh *et al.*, Nature (London) **452**, 970 (2008).
[7] D. Hsieh *et al.*, Nature (London) **460**, 1101 (2009).
[8] Y. Xia *et al.*, Nature Phys. **5**, 398 (2009).
[9] H. Zhang *et al.*, Nature Phys. **5**, 438 (2009).
[10] Y. L. Chen *et al.*, Science **325**, 178 (2009).
[11] D. Pesin and L. Balents, Nature Phys. **6**, 376 (2010).
[12] A. Shitade *et al.*, Phys. Rev. Lett. **102**, 256403 (2009).
[13] M. Liu *et al.*, Phys. Rev. B **83**, 165440 (2011).
[14] S. Raghu *et al.*, Phys. Rev. Lett. **100**, 156401 (2008).
[15] K. Sun, H. Yao, E. Fradkin, and S. A. Kivelson, Phys. Rev. Lett. **103**, 046811 (2009).
[16] M. Dzero, K. Sun, V. Galitski, and P. Coleman, Phys. Rev. Lett. **104**, 106408 (2010).
[17] S. Rachel and K. L. Hur, Phys. Rev. B **82**, 075106 (2010).
[18] C. N. Varney *et al.*, Phys. Rev. B **82**, 115125 (2010).
[19] A. Ström, H. Johannesson, and G. I. Japaridze, Phys. Rev. Lett. **104**, 256804 (2010); A. Ström and H. Johannesson, Phys. Rev. Lett. **102**, 096806 (2009).
[20] Z. Y. Meng *et al.*, Nature (London) **464**, 847 (2010).
[21] M. Hohenadler, T. C.Lang, and F. F. Assaad, Phys. Rev. Lett. **106**, 100403 (2011).
[22] D. Zheng, C. Wu, and G. M. Zhang, arXiv:1011.5858.
[23] M. Potthoff, Eur. Phys. J. B **32**, 429 (2003); M. Potthoff, M. Aichhorn, and C. Dahnken, Phys. Rev. Lett. **91**, 206402 (2003).
[24] D. Sénéchal *et al.*, Phys. Rev. Lett. **94**, 156404 (2005).
[25] M. Aichhorn *et al.*, Phys. Rev. B **74**, 024508 (2006).
[26] M. Balzer and M. Potthoff, Phys. Rev. B **82**, 174441 (2010).
[27] D. Sénéchal, and A.-M. S. Tremblay, Phys. Rev. Lett. **92**, 126401 (2004).
[28] C. Wu, B. A. Bernevig, and S. C. Zhang, Phys. Rev. Lett. **96**, 106401 (2006).
[29] C. Xu and J. E. Moore, Phys. Rev. B **73**, 045322 (2006).